Original Research Paper

Scavenger receptor A-mediated nanoparticles target M1 macrophages for acute liver injury

Rongping Zhang[a], Shiqing Luo[a], Ting Zhao[a], Mengying Wu[a], Lu Huang[a], Ling Zhang[b], Yuan Huang[a], Huile Gao[a], Xun Sun[a], Tao Gong[a,*], Zhirong Zhang[a]

[a] *Key Laboratory of Drug Targeting and Drug Delivery Systems, Ministry of Education, Sichuan University, Chengdu 610041, China*
[b] *College of Polymer Science and Engineering, Sichuan University, Chengdu 610041, China*

ARTICLE INFO

ABSTRACT

Acute liver injury (ALI) has an elevated fatality rate due to untimely and ineffective treatment. Although, schisandrin B (SchB) has been extensively used to treat diverse liver diseases, its therapeutic efficacy on ALI was limited due to its high hydrophobicity. Palmitic acid-modified serum albumin (PSA) is not only an effective carrier for hydrophobic drugs, but also has a superb targeting effect via scavenger receptor-A (SR-A) on the M1 macrophages, which are potential therapeutic targets for ALI. Compared with the common macrophage-targeted delivery systems, PSA enables site-specific drug delivery to reduce off-target toxicity. Herein, we prepared SchB-PSA nanoparticles and further assessed their therapeutic effect on ALI. *In vitro*, compared with human serum albumin encapsulated SchB nanoparticles (SchB-HSA NPs), the SchB-PSA NPs exhibited more potent cytotoxicity on lipopolysaccharide (LPS) stimulated Raw264.7 (LAR) cells, and LAR cells took up PSA NPs 8.79 times more than HSA NPs. As expected, the PSA NPs also accumulated more in the liver. Moreover, SchB-PSA NPs dramatically reduced the activation of NF-κB signaling, and significantly relieved inflammatory response and hepatic necrosis. Notably, the high dose of SchB-PSA NPs improved the survival rate in 72 h of ALI mice to 75%. Hence, SchB-PSA NPs are promising to treat ALI.

1. Introduction

One of the universal liver diseases worldwide, acute liver injury (ALI) can rapidly develop into life-threatening acute liver failure with limited treatment [1–3]. The hepatic macrophages, also called Kupffer cells, the most numerous immune cells in the liver, are situated in the hepatic sinusoids and provide a crucial function in varied liver diseases [4]. Particularly, M1 macrophages are essential for controlling the
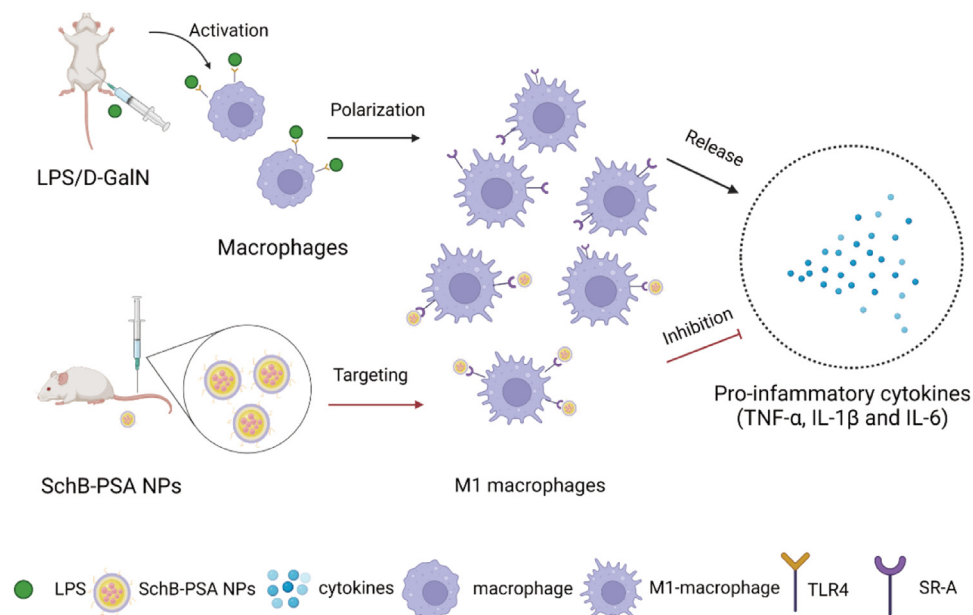
Scheme 1 – Schematic representation of the M1 macrophage targeting effect of SchB-PSA NPs on ALI. SchB-PSA NPs can specifically target SR-A overexpressed on M1 macrophages so that SchB can be released at sites of inflammation in the liver and inhibit the production of pro-inflammatory mediators to reduce liver injury.

inflammatory response in the organism [5–7], which is vital in the progression of ALI [5,8–12]. For ALI triggered by LPS/D-galactosamine (D-GalN), activated M1 macrophages release large amounts of pro-inflammatory cytokines containing the tumor necrosis factor α (TNF-α), interleukin-6 (IL-6) and IL-1β, which can aggravate the pathological progression and further lead to excessive hepatocyte death [5,13–15]. Therefore, the M1 macrophage is an attractive target for treating ALI.

Researchers have developed several kinds of strategies to target macrophages [16,17]. Among them, chondroitin sulfate (CS) and hyaluronic acid (HA) have been extensively used to modify nanoparticles (NPs) to target macrophages via CD44-mediated endocytosis [18,19]. However, the CD44 receptors are also expressed on erythrocytes, dendritic cells, endothelial cells, keratinocytes, et al. [20–22]. Although some studies also reported that mannose-modified NPs could target macrophages via mannose receptors [23], the mannose receptor is also found on various immune cells [24] and even on human keratinocytes [25]. These drug delivery systems could cause side effects due to unspecific site targeting. Accordingly, it is crucial to craft a specific target delivery system without impacting normal cells and tissues [26].

Scavenger receptors are highly expressed in the liver [27]. Specifically, the SR-A receptor, also named macrophage scavenger receptor 1 (MSR1) [28], is strongly and specifically expressed on activated macrophages, and its distribution in normal tissues is insignificant [29,30]. In our previous studies, Palmitic acid-modified serum albumin (PSA) NPs showed a more remarkable targeting effect on M1 macrophages via SR-A, which has been demonstrated to be stronger than the targeting effect of CS-modified NPs via CD44, whether *in vitro* or *in vivo* [29]. Therefore, the desirable property makes PSA a potential vehicle for treating ALI with desired efficacy and less toxicity.

Schisandrin B (SchB), isolated from *Schisandra Chinensis*, is a potential candidate compound for hepatic diseases, including acute liver injury [31], liver fibrosis [32,33], nonalcoholic fatty liver [34] and so on. And it has been documented to exhibit varieties of pharmacological actions, containing liver protection, antioxidant, anti-inflammation, antiaging and antitumor [35]. Mainly, SchB can prevent the activation of macrophages and the release of pro-inflammatory mediators by suppressing the nuclear factor κB (NF-κB) pathway [32,33,36–40]. The NF-κB signaling is essential for initiating an inflammatory response [41], and inflammation is a key pathological component of ALI [27]. Hence, SchB is an ideal drug for ALI. However, the effect of SchB is restricted due to its hydrophobicity and poor bioavailability via oral administration [42,43].

Here, PSA, a distinguished drug delivery carrier for hydrophobic drugs, was used to encapsulate SchB to improve its bioavailability and reduce toxicities. Small, stable, and well-dispersed SchB-PSA/HSA nanoparticles were prepared and characterized. The cytotoxicity and anti-inflammatory effect were evaluated *in vitro*. Then, we estimated the M1 macrophage targeting effect, distribution, and pharmacokinetic characteristics of PSA/HSA NPs *in vivo*. Ultimately, we evaluated the therapeutic actions of SchB-PSA NPs for treating ALI, in comparison to SchB-HSA NPs and SchB solution (Scheme 1).

2. Materials and method

2.1. Materials

Schisandrin B (SchB), N-succinimidyl palmitate (PA-NHSE) and D-galactosamine were obtained from Yuanye Bio-Technology Co., Ltd (Shanghai, China). Tieling Beiya pharmaceutical Oil Co., Ltd (Liaoning, China) provided medium chain triglyceride (MCT). Lipopolysaccharide (LPS) is from Biosharp (Hefei, China), while 1,19 -dioctadecyl-3,3,39,39 tetramethylindodicarbocyanine (DiD) from Biotium (Hayward, USA). ELISA kits used for assay of the levels of TNF-α, Il-6 and IL-1β. FITC-conjugated anti-rat F4/80 antibody and PE-conjugated anti-rat CD86 antibody were supplied by Invitrogen (CA, USA). Shanghai Bihe Biochemical Technology Co., Ltd offered an anti-CD204 (SR-A) antibody. The anti-CD86 antibody was from Abcam Shanghai Trading Co., Ltd. DAPI was from Beijing Solarbio Science & Technology Co., Ltd. Primary antibodies NFκB-p65, IκBα, phosphor-IκBα (p-IκBα), β-actin and secondary antibodies were from HuaBio Biotechnology Co., Ltd (Zhejiang, China), and phosphorylated NF-κB (p-p65) was from ImmunoWay Biotechnology Co., Ltd (DE, USA). All agents were of analytical grade or better.

2.2. Synthesis of PSA

PSA was synthesized as the previous reports [29,30]. Briefly, 6.6 g HSA powder was added to 20 ml NaHCO$_3$ buffer (pH 8.4–8.6) in a 37 °C water bath. Simultaneously 0.7 g PA-NHSE was added to 2 ml N, N-dimethylformamide in a 60 °C water bath, then immediately mixed with the HSA/NaHCO$_3$ solution and agitated at 37 °C water bath for 24 h. Finally, the mixed solution was dialyzed for 48 h at room temperature to remove the insoluble materials at 10,000 rpm for 10 min. Then PSA lyophilized powder was obtained by a freeze-dried method. Moreover, the PSA and HSA were characterized by circular dichroism and fluorescence spectra [29,30]. Briefly, PSA and HSA powder were dissolved in PBS (pH 7.27) to form 0.2 mg/ml solution, respectively. And the circular dichroism spectra was acquired via circular dichroism spectrometer (Chirascan, Applied Photophysics, UK) from 190 to 260 nm. The above solution was further diluted 4 times with PBS to obtain 0.05 mg/ml PSA and HSA solution, and the fluorescence spectra at the maximum excitation wavelength (Ex) of 280 nm was recorded via a fluorescence spectrophotometer (RF6000, SHIMADZU, Japan).

2.3. Preparation and characterization of SchB-PSA/HSA NPs

2.3.1. Preparation
SchB-PSA/HSA NPs were prepared [29,30]. 300 µl dichloromethane (Cdkelong, Chengdu, China) was used to dissolve SchB (10 mg) and MCT (35 mg). Subsequently, 5 ml PSA solution (15 mg/ml) was added. The mixed solution was sonicated at 220 W for 7 min (SCIENTZ-IID, Ningbo, China), and the residual dichloromethane was dismissed via rotary evaporation. The SchB-HSA NPs were obtained with HSA instead of PSA as described above. Meanwhile, for the biodistribution and cellular uptake studies, SchB was replaced by DiD to obtain the DiD-PSA NPs and DiD-HSA NPs.

2.3.2. Characterization
The Zetasizer Nano ZS90 instrument (Malvern Panalytical, Malvern, UK) was utilized for the measurement of particle sizes, polydispersity indexes (PDIs), and zeta potentials of SchB-PSA/HSA NPs. The transmission electron microscope (TEM, H-600, Hitachi, Japan) was employed to characterize the size and morphology of SchB-PSA/HSA NPs. Diluting the SchB-PSA/HSA NPs 10 times, they were put into the copper carrier net and stained with a 2% phosphotungstic acid solution. Moreover, the encapsulation efficiency (EE) and drug loading capacity (DLC) of both nanoparticles were determined using the ultrafiltration method, and computed respectively by Eqs. (1) and (2) [29,30]:

$$EE\ (\%) = \frac{\text{Weight of SchB loaded}}{\text{Weight of SchB added}} \times 100\% \tag{1}$$

$$DLC\ (\%) = \frac{\text{Weight of SchB loaded}}{\text{Weight of nanoparticles}} \times 100\% \tag{2}$$

2.3.3. Stability
The changes in particle sizes and PDIs were indicators to evaluate the stability of SchB-PSA/HSA NPs [29,30]. Firstly, to investigate the stability at different storage temperatures, SchB-PSA/HSA NPs were preserved at 4 °C or 37 °C for 7 d. Additionally, we investigated the dilution stability, plasma stability and serum stability of these nanoparticles. To evaluate the dilution stability, 1 ml SchB-PSA/HSA NPs were diluted 5, 10, 20, 50 and 100 times with water or PBS, respectively. To evaluate the stability in plasma and serum, PBS, plasma/serum and SchB-PSA/HSA NPs were well-mixed (1:1:1, v/v) in a thermostatic shaker (100 rpm, 37 °C) for 48 h.

2.4. Comparison of SchB-PSA/HSA NPs in vitro

Chinese Academy of Science Cell Bank (Shanghai, China) offered Raw264.7 cells (murine macrophages), which were grown in Dulbecco's modified Eagle medium (DMEM, BasalMedia, Shanghai, China), containing 10% fetal bovine serum (Lonsera, Shanghai, China), and 5% penicillin/streptomycin (Solarbio, Beijing, China) at 37 °C and 5% CO$_2$.

2.4.1. Cellular uptake
Raw264.7 cells (1 × 10^6 cells per well) were treated with/without 2 µg/ml LPS on 12-well plates for 24 h. Subsequently, the old medium was replaced with 1 ml fresh media containing DiD-PSA/HSA NPs (0.4 µg/ml DiD). After 2 h, cells were obtained, and analyzed by a NovoCyte Flow Cytometer (ACEA Biosciences, China).

Additionally, to intuitively investigate and compare the cellular uptake of two NPs, Raw264.7 cells were treated with or not 2 µg/ml LPS for 24 h in glass-bottomed dishes. The cells were incubated with DiD-PSA/HSA NPs diluted with the free-serum medium for another 1 h. Eventually, cells were

subjected to DAPI staining for 15 min at 37 °C [30]. The fluorescent images of Raw264.7 and LAR cells given DiD-PSA NPs or DiD-HSA NPs were obtained by a laser confocal microscope (CLSM, Zeiss, Germany).

2.4.2. Cell viability

The cell viability between different preparations was compared using the MTT assay [29,30]. LAR cells were activated M1 macrophages by the co-incubation of Raw264.7 cells and 2 µg/ml LPS for 24 h at 37 °C. Raw264.7 and LAR cells were placed in 96-well plates, and incubated with 100 µl of SchB-PSA NPs, SchB-HSA NPs and free SchB at serial concentration for 24 h. Afterwards, 100 µl MTT (0.5 mg/ml) in fresh free-serum media was added and reacted with viable cells to form formazan crystals, which were solubilized in dimethyl sulfoxide (DMSO). The absorbance at 490 nm of these plates was determined after shaking for 30 min (100 rpm, 37 °C). Cell viability was calculated using Eq. 3 [29,30].

$$\text{Cell viability (\%)} = \frac{\text{Atext} - \text{Ablank}}{\text{Acontrol} - \text{Ablank}} \times 100\% \qquad (3)$$

For the cell viability of blank PSA NPs, blank HSA NPs and DMSO, the blank carriers were added in the same volume as the SchB-PSA/HSA NPs and free SchB solution.

2.4.3. Anti-inflammatory effect of SchB-PSA/HSA NPs in vitro

LPS (100 ng/ml) was used to induce M1 macrophages [44], and then 15 µg/ml SchB-PSA/HSA NPs or SchB solution was added. Cells cultured in the media with or without LPS served as a positive control or a negative control group. The commercial ELISA kits were used to analyze the levels of TNF-α, IL-1β and IL-6 in the culture medium.

2.5. Establishment of liver injury model

6–7 weeks KM mice (30–32 g) were offered by Dashuo Experimental Animal, Inc. (Sichuan, China) and allowed to adjust to their surroundings for one week before the experiment. For the induction of ALI, mice were injected intravenously LPS (10 µg/kg) and D-GalN (700 mg/kg) for 1 h before the administration of different formulations [45]. All experiments in vivo were done under the guidelines confirmed by the Ethics Committee of Sichuan University.

2.6. M1 macrophages targeting effect of PSA NPs in vivo

We randomly divided 20 ALI mice into 4 groups (n = 5): DiD-PSA NPs, DiD-HSA NPs, free DiD and control. The control group of mice were administered saline intravenously, with the other group of mice receiving an intravenous injection of formulations at a dose of 200 µg/kg DiD. After 1.5 h, mice were sacrificed. The livers were soaked in polyformaldehyde for 48 h at room temperature and then made into 5 µm paraffin sections. The liver section in the control group was stained with anti-CD204 (SR-A), anti-CD86 antibody and DAPI according to the instructions to observe the co-localization of SR-A and M1 macrophages. The other liver sections in the preparation groups were stained with anti-CD204 (SR-

A) and DAPI to observe the co-localization of SR-A and DiD.

In addition, a flow cytometry was used to measure the uptake of DiD-PSA/HSA NPs by M1 macrophages of ALI mice. After the mice were sacrificed, $0.5 \times 0.5 \text{ cm}^2$ of the liver was triturated and filtered via a 70 µm cell strainer (Biosharp, China) to obtain cell suspension. Subsequently, non-parenchymal cells (NPCs) were obtained via centrifuging at 600 rpm for 8 min at 4 °C, and transferred to a new tube [46]. After centrifuging at 900 rpm for 8 min at 4 °C, the NPC pellet was obtained and mixed with 1 ml red blood cell lysis buffer (TBDscience, China) in an ice bath for 5 min [15]. The liver macrophages were extracted and stained with F4/80 and CD86 for 30 min at 4 °C. Cells were washed and finally suspended in 500 µl PBS. Finally, the cell suspension was filtered into a new flow tube, and analyzed on a flow cytometer [47].

2.7. Biodistribution study

By randomly assigning 54 ALI mice to three groups (n = 18), the biodistribution of DiD-PSA/ HSA NPs, and free DiD in ALI was carried out. These formulations were diluted with PBS to the same dose of 200 µg/kg DiD, and were administered intravenously for 1 h after the establishment of the ALI model. Mice were sacrificed at 2, 6 and 9 h after treatment with LPS/D-GalN, and the liver tissues were obtained and imaged through a Caliper in vivo imaging system Lumina III system (PerkinElmer, USA).

2.8. Pharmacokinetic study

200 ± 20 g male Sprague Dawley (SD) rats (Dashuo Experimental Animal, Inc.) were divided into 3 groups (n = 6). Respectively, SchB-PSA NPs, SchB-HSA NPs and free SchB were administered intravenously at the equivalent SchB dosage of 12 mg/kg. 400 µl blood samples were collected at pre-arranged time points (0.083, 0.25, 0.3, 1, 2, 4, 8, 12, 24, 36, 48 and 72 h), and then centrifuged at 3,000 rpm for 5 min to acquire the plasma supernatant. The liquid chromatography-mass spectrometry was used to measure the concentration of SchB [48].

2.9. In vivo therapeutic efficacy evaluation

The mice were divided randomly into 7 groups: LPS/D-GalN + 12 mg/Kg SchB-PSA NPs (H-SchB-PSA NPs), LPS/D-GalN + 8 mg/Kg SchB-PSA NPs (M-SchB-PSA NPs), LPS/D-GalN + 5 mg/Kg SchB-PSA NPs (L-SchB-PSA NPs), LPS/D-GalN + 12 mg/Kg SchB-HSA NPs (H-SchB-HSA NPs), LPS/D-GalN + 12 mg/Kg SchB solution (H-SchB Solution), LPS/D-GalN + saline and control. Mice in the control group were administered with sterile 0.9% saline rather than LPS/D-GalN. After 6 h post-administration of formulations, the animals were sacrificed (Fig. 6A). The liver tissues were obtained, washed and blotted dry with filter paper. The livers in all groups were fixed and stained with H&E. The liver histology score was evaluated by visualizing the entire H&E-stained section as described [14,49]. Briefly, we used a 0 (normal) to 3 (severe necrosis) scoring method to assess the condition of

liver injury ($n = 3$) [50]. What's more, the hepatic indexes ($n = 6$) were calculated after the fresh liver samples were weighted (Eq. 4) [51].

$$\text{Hepatic index} = \frac{\text{Fresh liver weight}}{\text{Mouse weight}} \qquad (4)$$

Meanwhile, the serum was obtained and centrifuged (6,000 rpm, 5 min) at 4 °C for further measurement. The TNF-α, IL-1, and IL-6 in the serum of formulations were analyzed by ELISA kits ($n = 6$). The concentration of serum aspartate aminotransferase (AST) and alanine aminotransferase (ALT) serve as indicators for the overall degree of liver injury, and were determined by the automatic biochemical analyzer (Roche Co., Ltd., Germany) ($n = 6$) [45]. Additionally, the mortality rates of all ALI mice were also recorded within 72 h ($n = 8$) [45].

2.10. Western blot analysis

After 6 h post-administration of formulations in ALI mice, we used the bicinchoninic acid (BCA) Kit (Dalian Meilun Biotechnology co., Ltd., Liaoning, China) to measure the concentration of total protein extracted in liver tissue. 30 µg protein was separated and transferred to polyvinylidene fluoride membranes [52]. These membranes were treated with primary antibodies containing p-p65 (1:900), p65 (1:1,000), p-IκBα (1:800), IκBα (1:3,500) and β-actin (1:5,000), and then incubated for 1 h with secondary antibodies (1:20,000). The enzyme-linked chemiluminescence (Thermo Fisher, MA, USA) was used to visualize the antibody binding in the membranes, which was observed using ImageJ software (National Institutes of Health, Bethesda, USA).

2.11. Proportion of M1 macrophages in the liver

Liver macrophages were extracted 6 h after intravenous administration of SchB to ALI mice. The liver macrophages were stained with anti-F4/80 and anti-CD86 antibody. A flow cytometer was used to observe the percentage of M1 macrophages in the liver after the treatment of SchB-containing formulations.

2.12. Statistical analysis

The quantitative data were shown as average ± standard deviation (SD). Each experiment was implemented at least three times. Non-linear regression in Drug and Statistics software 2.0 (Mathematical Pharmacology Professional Committee of China, Shanghai, China) was used to figure out the pharmacokinetic parameters. A one-way analysis of variance (ANOVA) and student's t-test were used to evaluate differences between numerous groups and two groups with GraphPad Prism 6.0 (GraphPad, CA, USA), and $P < 0.05$ was considered to be statistically significant.

3. Result and discussion

3.1. Property and stability of SchB-PSA/HSA NPs

As reported in previous studies [29,30], PSA was synthesized by the reaction between the lysine residue in HSA and PA-NHSE (Fig. 1B). The circular dichroism spectrum showed that PSA and HSA had altered secondary structure. The maximum emission wavelengths (Em) in the fluorescence spectrum of PSA and HSA were respectively at 315 nm and 334 nm (Fig. S1). The blue-shifted Em of PSA is due to its hydrophobic environment [29]. The results are consistent with our earlier findings [29,30], and also prove the successful synthesis of PSA.

The characteristics of the SchB-PSA/HSA NPs are exhibited in Table 1. PDIs of the SchB-PSA and SchB-HSA NPs were 163.3 nm (0.12) and 170.2 nm (0.06), respectively. TEM consistently showed that PSA had smaller particle sizes (Fig. 2A and 2B). The average zeta potentials of SchB-PSA NPs and SchB-HSA NPs were −37.3 mV and −15.4 mV (Fig. S2). PSA exhibited a more negative charge because the amino groups in PSA were lesser than that of HSA. Additionally, the blank PSA/HSA NPs and the DiD-PSA/HSA NPs had similar sizes, PDIs and zeta potentials as corresponding drug-loaded nanoparticles (Fig. S3), indicating that loading SchB or DiD did not affect the properties of PSA or HSA NPs and DiD-encapsulated NPs can be used for cellular uptake, *in vivo* distribution and other experiments. Moreover, the hydrophobicity of PSA makes it possible to encapsulate
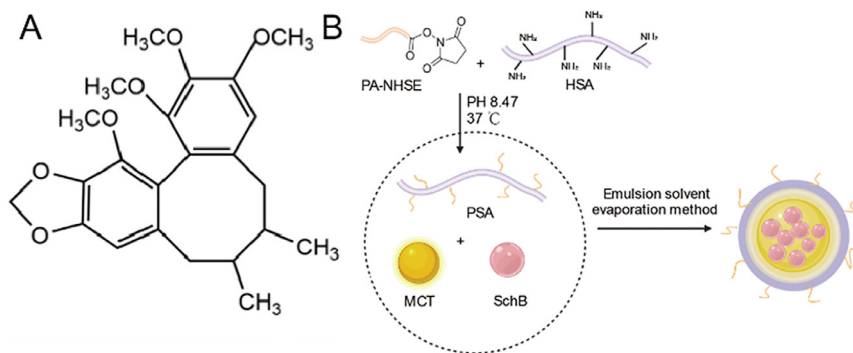
Fig. 1 – Schematic illustration of the formation of SchB-PSA NPs. SchB chemical structure (A), and the preparation of PSA and SchB-PSA NPs (B).

Table 1 – Characteristics of SchB-PSA/HSA NPs (mean ± SD, *n* = 3).

Nanoparticles	Size(nm)	PDIs	Zeta potential (mV)	EE (%)	DLC (%)
SchB-PSA NPs	163.3 ± 1.3	0.12±0.04	−37.3 ± 1.4	98.2 ± 0.9	5.90 ± 0.23
SchB-HSA NPs	170.2 ± 3.6	0.06±0.01	−15.4 ± 0.4	94.8 ± 1.0	4.78 ± 0.10
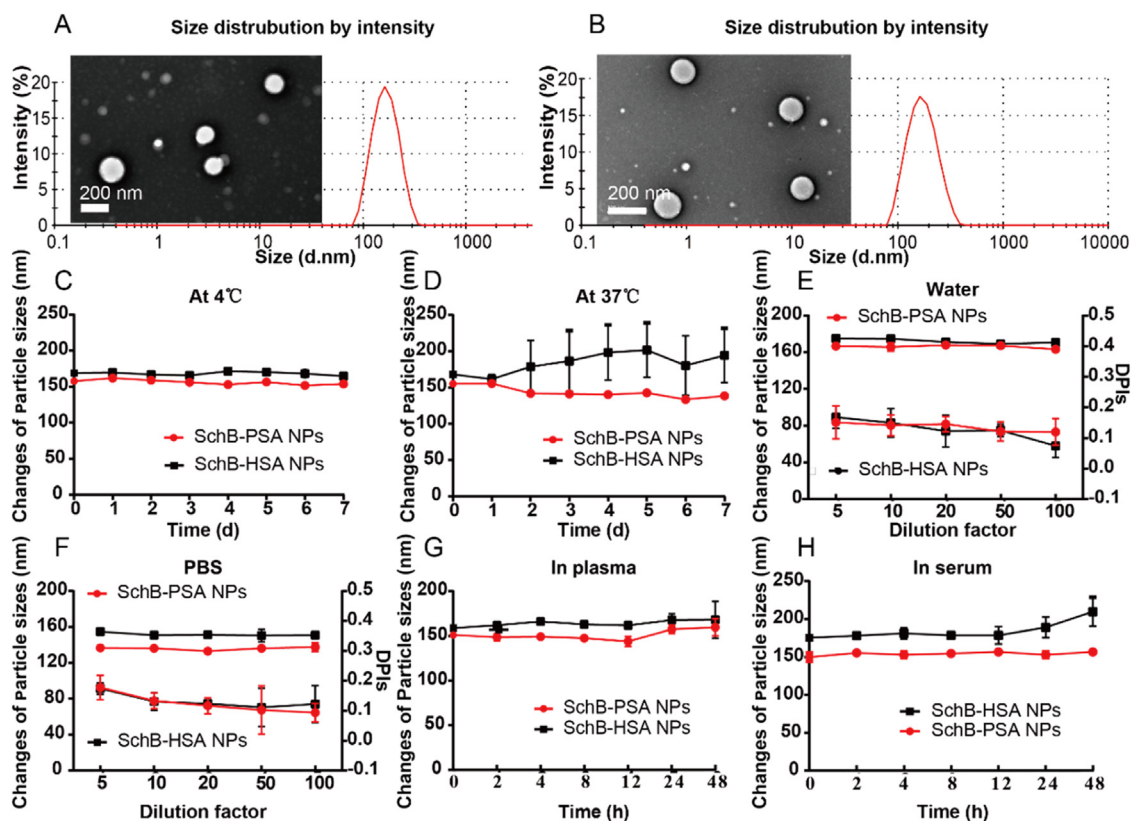
Fig. 2 – Physicochemical properties of the SchB-PSA/HSA NPs (*n* = 3). PDI and TEM of SchB-PSA (A) or SchB-HSA NPs (B). Storage stability of SchB-PSA/HSA NPs at 4 °C (C) or 37 °C (D). The dilution stability of SchB-PSA/HSA NPs in water (E) or PBS (F). The stability of SchB-PSA/HSA NPs in plasma (G) or serum (H) for 48 h.

SchB better, and SchB-PSA NPs showed slightly higher EE (98.2% *vs* 94.8%) and DLC than SchB-HSA NPs (5.90% *vs* 4.78%).

Although the changes of both NPs in particle sizes and PDIs at 4 °C for 7 d were negligible, the particle sizes of SchB-HSA NPs at 37 °C increased by 40 nm (Fig. 2C& 2D and S4). These datas indicate that SchB-PSA NPs have better stability under long-term storage conditions at 4 °C or 37 °C, compared with SchB-HSA NPs. The dilution stability is critical to avoid nanoparticle disassembly and drug unloading after intravenous injection [53]. Our studies showed that SchB-PSA NPs and SchB-HSA NPs exhibited excellent dilution stability in water or PBS (Fig. 2E and 2F). Meanwhile, interactions with serum protein may induce the premature release of drugs from NPs before they reach their target sites [53–55]. Therefore, we studied the plasma and serum stability of SchB-PSA/HSA NPs. They showed excellent stability in plasma or serum over 48 h. However, the size of SchB-HSA NPs increased by 34.1 nm at 48 h in serum, and the PDIs were more than 0.3 in plasma

and serum (Fig. 2G & 2H and S4). These stabilities suggest that SchB-PSA NPs may be more stable than SchB-HSA NPs after entering circulation, which is essential for intravenous drug delivery systems [53].

As previously reported [29,30], the *α*-helix makes the structure of PSA tighter and more stable. And PSA is more hydrophobic than HSA to form more compact and stable NPs with the hydrophobic drug. The factors above explain why SchB-PSA NPs show smaller particle sizes, higher EE and DLC, and more outstanding stabilities than SchB-HSA NPs.

3.2. Cell experiment of SchB-PSA/HSA NPs

3.2.1. Cellular uptake
To induce Raw264.7 cells to polarize into M1 macrophages, 2 µg/ml LPS was added [29,52]. After the stimulation of LPS, the cell morphology changed from cobblestone to spindle-shaped (Fig. S5). Raw264.7 took up DiD-PSA NPs about 3.77 times greater than DiD-HSA NPs. Notably, LAR took DiD-PSA
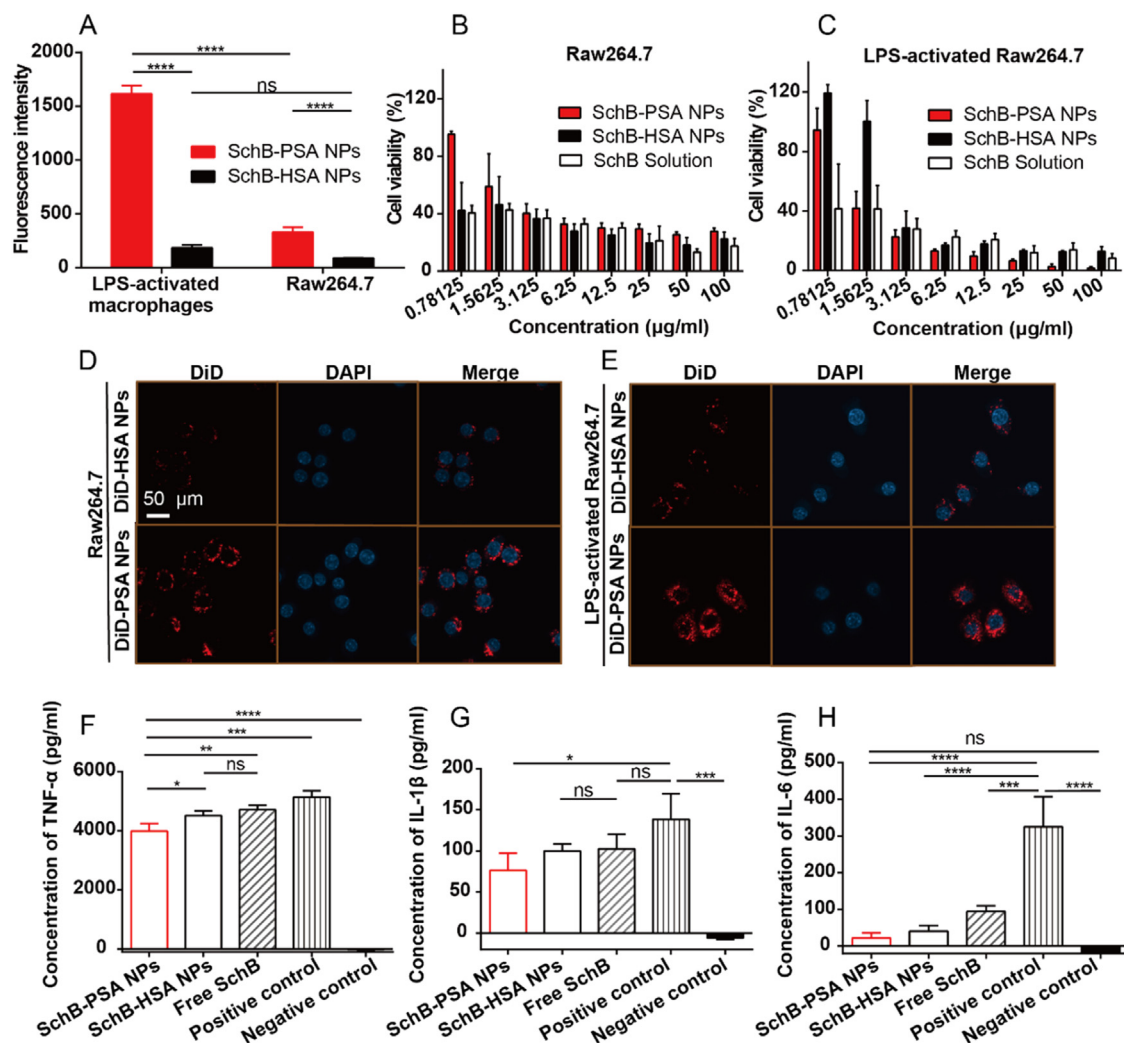
Fig. 3 – The cellular uptake of DiD-PSA/HSA NPs on Raw264.7 and LPS-activated macrophages for 2 h (A) (*n* = 3); Cytotoxicity of SchB -PSA NPs, SchB -HSA and SchB solution on Raw264.7 (B) and LAR (C) (*n* = 6); Confocal images of DiD-PSA/HSA NPs on Raw264.7cells (D) and LAR (E) (*n* = 3). Red: DiD; Blue: DAPI. Scale bar = 50 μm; Effects of SchB-PSA NPs, SchB-HSA NPs and SchB solution on the generation of TNF-*α* (F), IL-1*β* (G) and IL-6 (H) on LAR cells. The concentration of these cytokines in the negative control group is below the standard curve. *P < 0.05, ** P < 0.01, *** P < 0.001, and **** P < 0.0001. NS: no significance.

NPs around 8.79 times greater than the DiD-HSA NPs (Fig. 3A). Consistently, the laser confocal microscopy also showed that DiD-PSA NPs had higher uptake in LAR (Fig. 3D and 3E). These results provide strong evidence for the targeting effect of PSA NPs for M1 macrophages.

3.2.2. Cytotoxicity

The cytotoxicity of all formulations was dose-dependent according to the MTT assay. At almost all concentrations tested, there was no difference between the cytotoxicity of free SchB in the two cell types, indicating that SchB is a potent compound with no selectivity between Raw264.7 and LAR. Meanwhile, SchB-HSA NPs exhibited more significant cytotoxicity in Raw264.7 cells than SchB-PSA NPs (Fig. 3B). However, SchB-PSA NPs exhibited more significant cytotoxicity in LAR than SchB-HSA NPs (Fig. 3C), showing that

SchB-PSA NPs have selectivity against M1 macrophages. Next, we explored the cytotoxicity of blank NPs on macrophages (Fig. S6). The blank PSA NPs, blank HSA NPs, or DMSO solution had little cytotoxic effects with high viability on two types of cells (>85%). All these results indicated that SchB-PSA NPs could significantly eliminate M1 macrophages than SchB-HSA NPs.

3.2.3. Anti-inflammatory effect of SchB-PSA/HSA NPs in vitro

Among these formulations, SchB-PSA NPs obviously restrained the production of TNF-*α*, IL-1*β* and IL-6. Although SchB-HSA NPs also suppressed these inflammatory factors, there was no significant difference between SchB-HSA NPs and free SchB solution for TNF-*α* and IL-1*β* production (Fig. 3F–3H).

3.3. M1 macrophage targeting effect in vivo

The fluorescence of CD86 and CD204 was almost completely overlaid, which illustrates that SR-A is highly expressed on M1 macrophages in ALI mice (Fig. 4A) [29]. The confocal microscopy also showed that DiD-PSA NPs localized to SR-A. At the same time, only a small number of DiD-HSA NPs and a minimal number of free DiD overlapped with SR-A (Fig. 4B). These results demonstrate that PSA NPs target M1 macrophages via SR-A so that PSA NPs could be taken up by M1 macrophages.

The M1 macrophages were isolated from the liver of ALI mice, and then we assessed the uptakes of DiD-PSA/HSA NPs using a flow cytometry. As shown in Fig. 4C, the uptake of DiD-PSA NPs was 1.90 and 4.20 times higher than that of DiD-HSA NPs and free DiD, which further exhibits the targeting ability of PSA NPs on M1 macrophages.

3.4. Pharmacokinetics and biodistribution of NPs in vivo

SchB-PSA NPs exhibited the highest peak plasma concentration, the larger area under the curve (AUC), and the longest circulation time (Fig. 5A and 5B). The AUC_{0-t} of SchB-PSA NPs was 1.53 and 2.46 times higher than that of SchB-HSA NPs and free SchB solution. Moreover, the half-time of SchB-PSA NPs has been prolonged by about 13 h, compared with the free SchB solution. These results demonstrate that the circulation time could be prolonged and the bioavailability could be improved with SchB-PSA NPs compared with HSA NPs, which is due to the stabilities of SchB-PSA NPs [29,30].

Next, in vivo imaging system was used to estimate the distribution of the DiD-PSA/HSA NPs in ALI mice. DiD-PSA NPs exhibited stronger fluorescence intensity in the liver at different time intervals than DiD-HSA NPs (Fig. 5C). Even the semiquantitative analysis of liver tissues at 9 h displayed that the DiD-PSA NPs exhibited stronger fluorescence intensity, which was 2.89 and 3.29 times than that of DiD-HSA NPs and DiD group (Fig. 5D–5F). These results confirm that PSA NPs could achieve more accumulation and longer retention in the liver on ALI mice than HSA NPs due to the M1 macrophage targeting effect and extended SchB circulation time.

3.5. Therapeutic efficacy of SchB-PSA/HSA NPs

LPS/D-GalN-caused ALI has similar pathogenesis to human fulminant hepatitis [14]. Therefore, LPS/D-GalN has been commonly used to induce ALI for laboratory animal models [8,13,32,43,56]. There were inflammatory infiltration, destruction of liver cells, congestion of the liver, and a high mortality rate in ALI mice [2,50]. Conventional treatment indicators include the H&E staining, the hepatic index, the levels of AST and ALT, and the survival rates.

After establishing the ALI model according to the process diagram (Fig. 6A), severe liver congestion could be observed in all moribund or dead ALI mice [51]. The gross examination of the liver showed that LPS/D-DalN induced severe congestion in the saline group, and the high-dose SchB-PSA NPs could reduce the degree of congestion in liver tissues (Fig. 6B). Meanwhile, the H&E staining images of liver tissues were assessed according to the method described

[48,51]. We observed extensive hepatic damage and significant inflammatory cell infiltration in the ALI mice. And the high-dose SchB-PSA NPs could significantly decrease the degree of hepatocellular necrosis (Fig. 6C and 6D). Moreover, liver weights were raised because of liver congestion (Fig. 6E). The mice in the saline group had a higher hepatic index than the other ALI mice. However, the hepatic index in the high-dose SchB-PSA NPs was the lowest in all ALI mice. All these results display that PSA NPs have a preeminent efficacy on reducing the necrosis in hepatocytes, the number of inflammatory cells, and the congestion of the liver.

Some researches demonstrate that TNF-α, IL-1β and IL-6 are vital for the progression of ALI [14,57-59]. These cytokines regulate the inflammatory process and cause apoptosis, liver damage, and even death in ALI [50,57]. Especially, TNF-α is regarded as the leading cytokine that causes the mortality of ALI caused by LPS/D-GalN [50]. Therefore, the levels of these inflammatory cytokines are indicators for treating ALI. To further compare the anti-inflammatory action of SchB-PSA/HSA NPs in vivo, inflammatory factors above in the serum were measured by ELISA (Fig. 6F–6H). The concentration of inflammatory factors was considerably lowered after the treatment of high-dose of SchB-PSA NPs. Especially, the medium-dose of PSA NPs had a more powerful inhibitory effect on the release of TNF-α and IL-1β than high-dose HSA NPs. Furthermore, the low-dose PSA NPs showed better inhibition of the generation of IL-6 than the SchB solution.

The serum AST and ALT concentrations are often related to the condition of liver injury [60]. The sharp rise in AST and ALT values 6 h after the establishment of the animal ALI model suggested the emergence of acute liver failure [43]. The results exhibited that serum AST and ALT values of ALI mice given high-dose SchB-PSA NPs were significantly reduced to near the normal level, compared with other ALI mice (Fig. 6I and 6J), which is consistent with the histopathological examination and the levels of inflammatory factors.

Rapidly progressing hepatic failure is the cause of the high lethality of ALI mice induced by LPS/D-GalN [49]. Sudden death commonly occurred within 10 h, and no ALI mice could survive within 24 h. However, the survival rate was improved to 75% in the high-dose SchB-PSA NPs group in 72 h (Fig. 6K). The survival rate of the medium-dose and low-dose SchB-PSA NPs was 37.5%, while the survival rate of the high-dose SchB-HSA NPs was 25%. All the mice given high-dose SchB solution died at 48 h, and the mice in the saline group all died at 30 h.

These results indicate that SchB-PSA NPs have a potent therapeutic effect on ALI. High-dose SchB-PSA NPs are more effective than high-dose SchB-HSA NPs and high-dose free SchB solution on ALI mice. Medium-dose SchB-PSA NPs are also more effective than high-dose SchB-HSA NPs, and low-dose SchB-PSA NPs even have a better treatment effect than high-dose SchB solution. This prominent therapeutic effect of PSA NPs is closely related to the slow-release effect of SchB-PSA NPs and the ability to target M1 macrophages. SchB-PSA NPs could extend the circulation time of SchB and promote the uptake of SchB by M1 macrophages via SR-A, thus enhancing the accumulation of SchB in M1 macrophages in the liver. Hence, PSA NPs could effectively reduce liver inflammation, ameliorate liver damage and prolong survival in ALI mice.
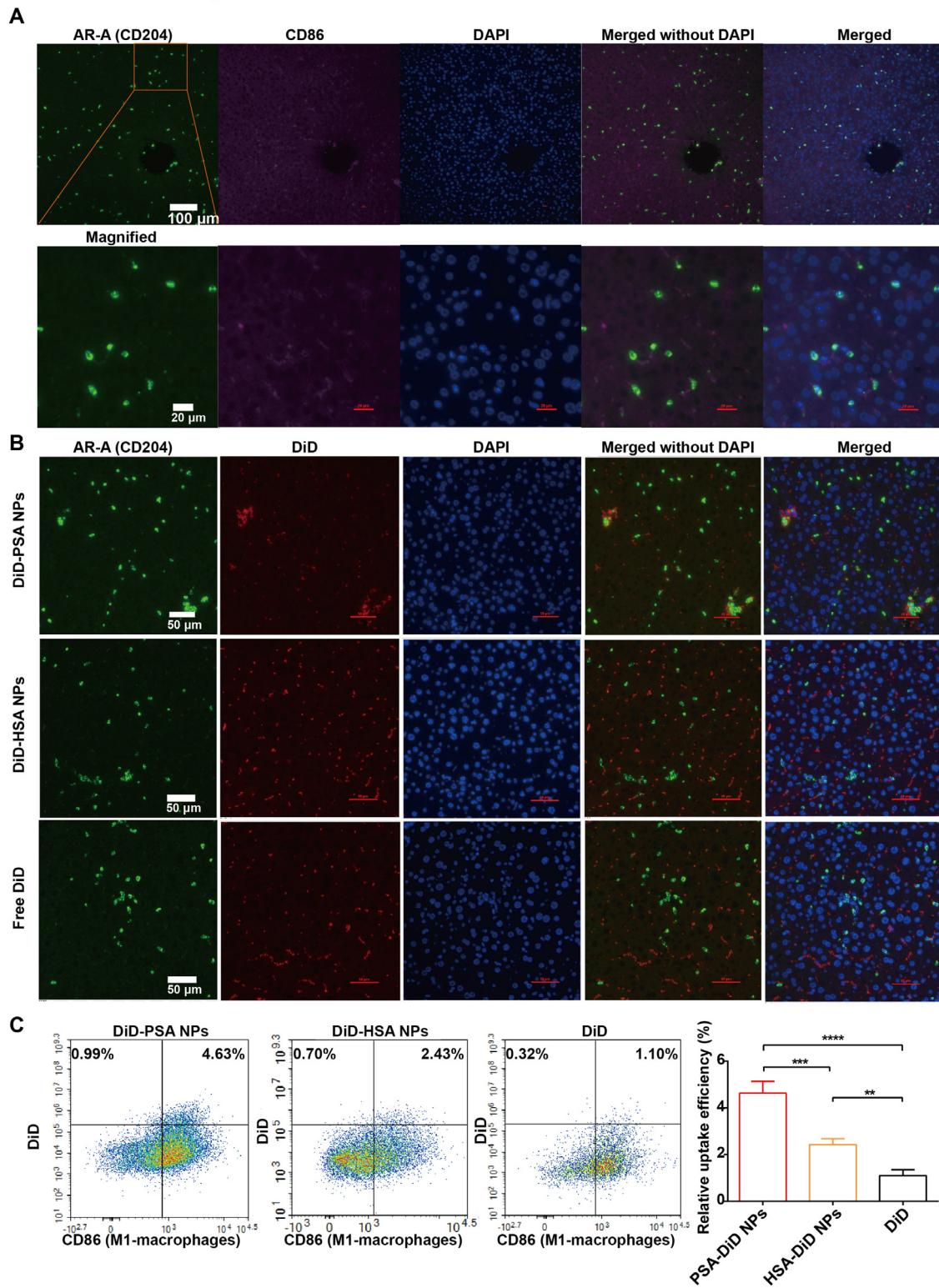
Fig. 4 – The M1 macrophages targeting effect of PSA NPs *in vivo* (*n* = 5). (A) The co-localization of SR-A (red) and M1 macrophages (purple). Scale bar: 100 µm. (B) Confocal micrographs of DiD-PSA NPs, DiD-PSA NPs and free DiD in the liver of ALI mice. Green: SR-A, Red: DiD, Blue: DAPI. Sclar bar = 50 µm. (C) Cellular uptake of DiD-PSA NPs, DiD-PSA NPs and free DiD by M1 macrophages. *P < 0.05, **P < 0.01, ***P < 0.001, and ****P < 0.0001. NS: no significance.
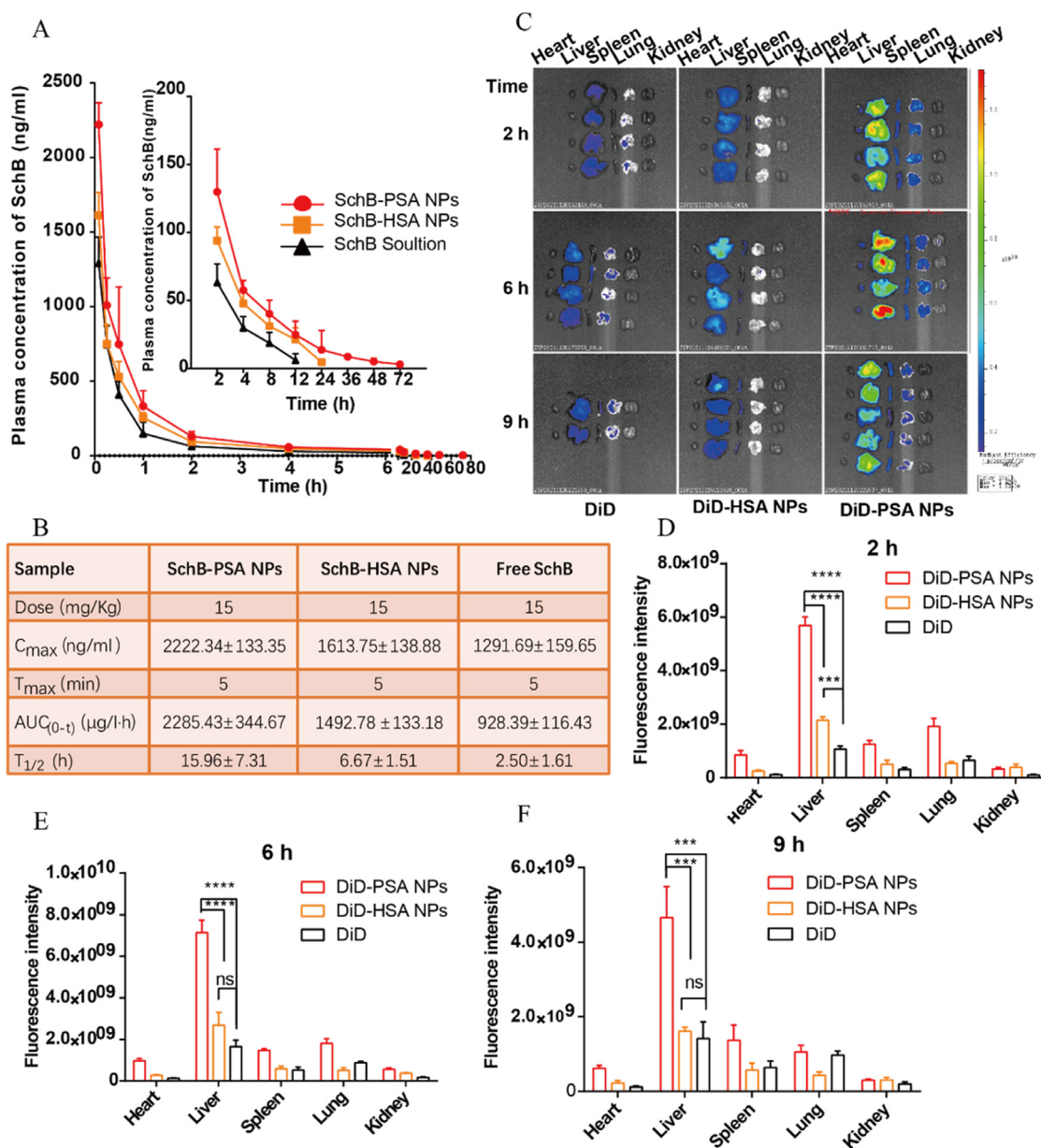
Fig. 5 – *In vivo* experiments of SchB-PSA/HSA NPs. The drug concentration-time curve (A) and parameters (B) of SchB-PSA NPs, SchB-HSA NPs and free SchB ($n = 6$); The *ex vivo* imaging in the liver after the administration of DiD-PSA NPs, DiD-HSA NPs and free DiD during different time intervals (C). The fluorescence analysis of the liver at 2 h (D), 6 h (E) and 9 h (F) in different groups. *$P < 0.05$, **$P < 0.01$, ***$P < 0.001$, and ****$P < 0.0001$. NS: no significance.

3.6. Mechanism of SchB-PSA NPs treating ALI

LPS induced-M1 macrophage polarization via binding to toll-like receptor (TLR)−4 after the administration of LPS/D-GalN [61]. IκBα was phosphorylated and subsequently contributed to the phosphorylation of NF-κB [62]. NF-κB activation can result in the production of pro-inflammatory cytokines, and the polarization of M1 macrophages, which can ultimately create severe liver damage [36,63–65]. Consequently, suppressing NF-κB activation is an encouraging strategy for treating ALI [66]. We further studied the phosphorylation of NF-κB and IκBα by Western blot ($n = 3$) (Fig. 7A–7C, and

S7). The outcomes demonstrated that LPS/D-DalN could promote the expression of p-p65 and p-IκBα. In particular, the inhibitory effect of PSA NPs was dose-dependent, and the expression levels of two phosphorylated proteins were significantly reduced to the same extent as the saline group after treating high-dose SchB-PSA NPs. Medium-dose SchB-PSA NPs had a comparable level of p-p65 with the high-dose SchB-HSA NPs, and the expression level of p-IκBα of the former was even lower than the latter. The p-p65 and p-IκBα of low-dose SchB-PSA NPs were less expressed than that in high-dose SchB solution. The remarkable SR-A targeting effect enables rapid and massive uptake of SchB-PSA NPs
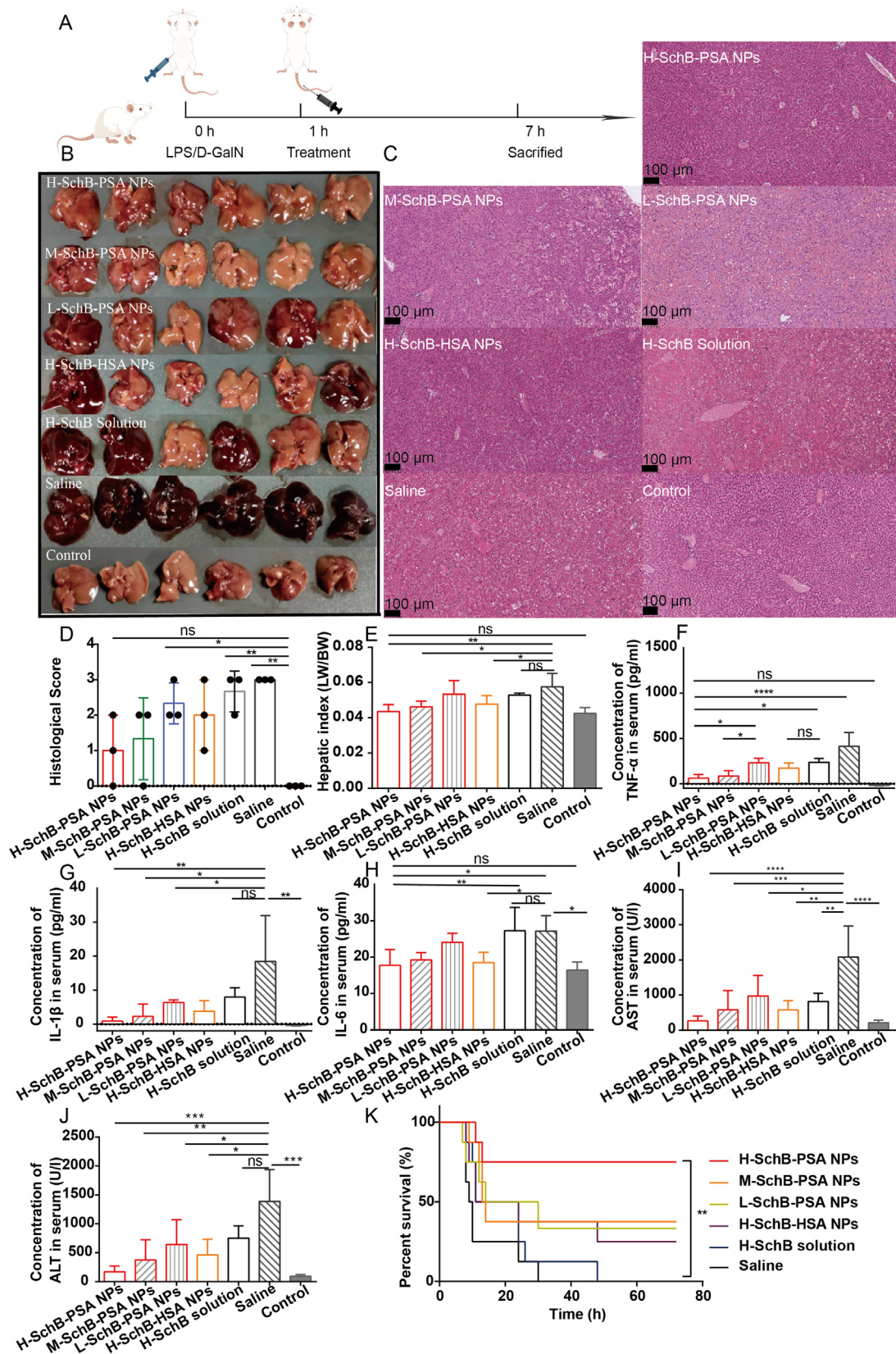
Fig. 6 – The effects of different formulations against ALI. The diagrammatic figure of the LPS/D-GalN-induced ALI model (A). The gross examination of the liver (B), H&E staining of liver sections (C), histological scores (D) and hepatic index (E) under different treatment conditions, Scale bar: 100 μm. Serum TNF-α (F), IL-1β (G) and IL-6 (H), AST (I) and ALT (J) levels of ALI mice were analyzed. Survival curves of ALI mice in 72 h (K). *$p < 0.05$, **$p < 0.01$, ***$p < 0.001$, and ****$p < 0.0001$. NS: no significance.
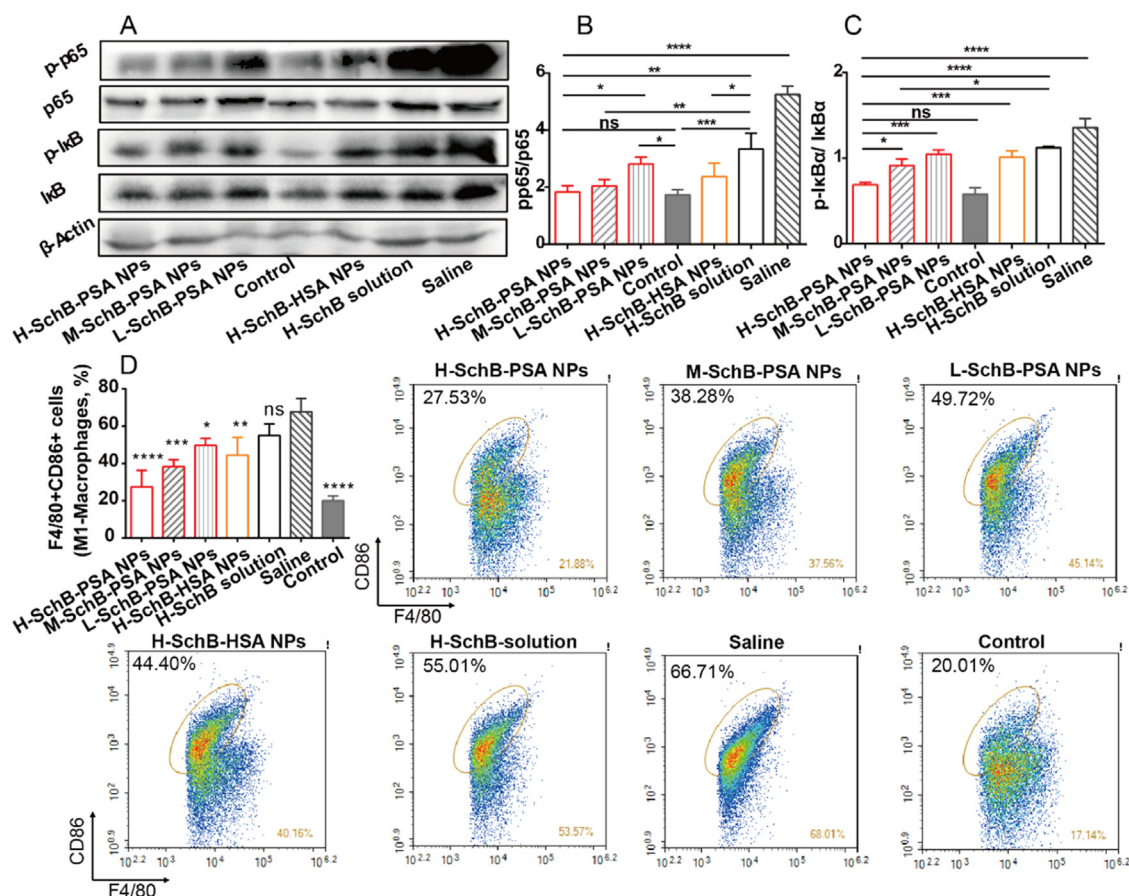
Fig. 7 – The mechanisms of SchB-PSA NPs in ALI mice. Total protein in liver tissues was analyzed by Western blotting (A). The densitometric analysis was used to quantify the expression of p-p65, p65, p-IκBα and IκBα (B-C) ($n = 3$). The rate of M1 macrophages was measured by flow cytometry (D) ($n = 6$) *$P < 0.05$, **$P < 0.01$, ***$P < 0.001$, and ****$P < 0.0001$. NS: no significance.

by activated M1 macrophages so that SchB-PSA NPs could efficiently suppress the phosphorylation of NF-κB and IκBα in ALI mice, compared with SchB-HSA NPs and free SchB.

Consistently, the flow cytometry showed that the SchB-PSA NPs exhibited a notable effect on reducing the expressions of M1 macrophages. The SchB-PSA NPs and SchB-HSA NPs decreased the percentage of M1 macrophages in the liver to 27.53% and 44.40%, while the proportion of healthy mice was 20.01% (Fig. 7D). Inhibition of the activation of M1 macrophage is essential to reduce inflammation in the liver. PSA delivered SchB to activated M1 macrophages in ALI mice, and efficiently prevented the activation of M1 macrophages. Therefore, SchB-PSA NPs have outstanding therapeutic effects against ALI.

These results prove that SchB-PSA NPs are attractive for the treatment of ALI due to suppressing the activation of M1 macrophage through down-regulating the NF-κB signaling pathway.

4. Conclusion

In order to overcome the drawbacks of the current macrophage-targeted drug delivery systems, PSA was used to encapsulate SchB in this study. Compared with HSA NPs, PSA NPs not only had excellent stabilities and superior drug delivery performance but also showed a potent targeting effect on activated M1 macrophages in vitro and in vivo. In vitro, PSA NPs displayed potent cytotoxicity and outstanding anti-inflammatory action. In vivo, the remarkable targeting effect on M1 macrophages and the prolonged circulation time of SchB-PSA NPs made them accumulate more in the liver of ALI mice and achieved a better treatment effect. The SchB-PSA NPs reduced the production of pro-inflammatory cytokines and diminished the number of M1 macrophages to near the average level via downregulating the NF-κB pathway. Therefore, SchB-PSA NPs effectively controlled the inflammatory response in the liver and reduced liver damage in ALI mice.

All in all, these discoveries demonstrate that PSA has prominent targeting of M1 macrophages, thus making it a viable vehicle for treating the acute liver injury. Meanwhile, M1 macrophages are essential cells involved in the pathological process of diverse liver diseases, and SchB is a promising candidate to treat liver diseases. Hence, SchB-PSA NPs may hold great promise for treating various liver diseases.

Conflicts of interest

The authors have declared that no conflict interests exist.

Acknowledgments

Supplementary materials

Supplementary material associated with this article can be found, in the online version, at doi:10.1016/j.ajps.2023.100813.

REFERENCES

[1] Reuben A, Tillman H, Fontana RJ, Davern T, McGuire B, Stravitz RT, et al. Outcomes in adults with acute liver failure between 1998 and 2013: an observational cohort study. Ann Intern Med 2016;164(11):724–32.

[2] Mao J, Yi M, Wang R, Huang Y, Chen M. Protective effects of costunolide against D-galactosamine and lipopolysaccharide-induced acute liver injury in mice. Front Pharmacol 2018;9:1469.

[3] Mauro E, Garcia-Olveira L, Gadano A. End-stage liver disease: management of hepatorenal syndrome. Liver Int 2021;41(Suppl 1):119–27.

[4] Wen Y, Lambrecht J, Ju C, Tacke F. Hepatic macrophages in liver homeostasis and diseases-diversity, plasticity and therapeutic opportunities. Cell Mol Immunol 2021;18(1):45–56.

[5] Tacke F. Targeting hepatic macrophages to treat liver diseases. J Hepatol 2017;66(6):1300–12.

[6] Hu G, Guo M, Xu J, Wu F, Fan J, Huang Q, et al. Nanoparticles targeting macrophages as potential clinical therapeutic agents against cancer and inflammation. Front Immunol 2019;10:1998.

[7] Lu HL, Huang XY, Luo YF, Tan WP, Chen PF, Guo YB. Activation of M1 macrophages plays a critical role in the initiation of acute lung injury. Biosci Rep 2018;38(2):20171555.

[8] Yang W, Tao K, Zhang P, Chen X, Sun X, Li R, et al. Maresin 1 protects against lipopolysaccharide/d-galactosamine-induced acute liver injury by inhibiting macrophage pyroptosis and inflammatory response. Biochem Pharmacol 2022;195:114863.

[9] Tsutsui H, Nishiguchi S. Importance of Kupffer cells in the development of acute liver injuries in mice. Int J Mol Sci 2014;15(5):7711–30.

[10] Antoniades CG, Quaglia A, Taams LS, Mitry RR, Hussain M, Abeles R, et al. Source and characterization of hepatic macrophages in acetaminophen-induced acute liver failure in humans. Hepatology 2012;56(2):735–46.

[11] Xia Y, Wang P, Yan N, Gonzalez FJ, Yan T. Withaferin A alleviates fulminant hepatitis by targeting macrophage and NLRP. Cell Death Dis 2021;12(2):174.

[12] Zimmermann HW, Trautwein C, Tacke F. Functional role of monocytes and macrophages for the inflammatory response in acute liver injury. Front Physiol 2012;3:56.

[13] Liu Y, Liu N, Liu Y, He H, Luo Z, Liu W, et al. Ginsenoside Rb1 reduces D-GalN/LPS-induced acute liver injury by regulating TLR4/NF-κB signaling and NLRP3 inflammasome. J Clin Transl Hepatol 2022;10(3):474–85.

[14] Lv H, Qi Z, Wang S, Feng H, Deng X, Ci X. Asiatic acid exhibits anti-inflammatory and antioxidant activities against lipopolysaccharide and D-galactosamine-induced fulminant hepatic failure. Front Immunol 2017;8:785.

[15] Daemen S, Chan MM, Schilling JD. Comprehensive analysis of liver macrophage composition by flow cytometry and immunofluorescence in murine NASH. STAR Protoc 2021;2(2):100511.

[16] Ponzoni M, Pastorino F, Di Paolo D, Perri P, Brignole C. Targeting macrophages as a potential therapeutic intervention: impact on inflammatory diseases and cancer. Int J Mol Sci 2018;19(7):1953.

[17] Jain NK, Mishra V, Mehra NK. Targeted drug delivery to macrophages. Expert Opin Drug Deliv 2013;10(3):353–67.

[18] Xu H, Luo R, Dong L, Pu X, Chen Q, Ye N, et al. PH/ROS dual-sensitive and chondroitin sulfate wrapped poly (β-amino ester)-SA-PAPE copolymer nanoparticles for macrophage-targeted oral therapy for ulcerative colitis. Nanomedicine 2022;39:102461.

[19] Gou S, Huang Y, Wan Y, Ma Y, Zhou X, Tong X, et al. Multi-bioresponsive silk fibroin-based nanoparticles with on-demand cytoplasmic drug release capacity for CD$_{44}$-targeted alleviation of ulcerative colitis. Biomaterials 2019;212:39–54.

[20] Park JW, Jung KH, Lee JH, Moon SH, Cho YS, Lee KH. ^{89}Zr anti-CD$_{44}$ immuno-PET monitors CD$_{44}$ expression on splenic myeloid cells and HT$_{29}$ colon cancer cells. Sci Rep 2021;11(1):3876.

[21] Hu JB, Li SJ, Kang XQ, Qi J, Wu JH, Wang XJ, et al. CD$_{44}$-targeted hyaluronic acid-curcumin prodrug protects renal tubular epithelial cell survival from oxidative stress damage. Carbohydr Polym 2018;193:268–80.

[22] Jordan AR, Racine RR, Hennig MJ, Lokeshwar VB. The role of CD$_{44}$ in disease pathophysiology and targeted treatment. Front Immunol 2015;6:182.

[23] Wei Z, Huang L, Cui L, Zhu X. Mannose: good player and assister in pharmacotherapy. Biomed Pharmacother 2020;129:110420.

[24] Azad AK, Rajaram MV, Schlesinger LS. Exploitation of the macrophage mannose receptor (CD206) in infectious disease diagnostics and therapeutics. J Cytol Mol Biol 2014;1(1):1000003.

[25] Szolnoky G, Bata-Csörgö Z, Kenderessy AS, Kiss M, Pivarcsi A, Novák Z, et al. A mannose-binding receptor is expressed on human keratinocytes and mediates killing of Candida albicans. J Invest Dermatol 2001;117(2):205–13.

[26] Zhao Z, Ukidve A, Kim J, Mitragotri S. Targeting strategies for tissue-specific drug delivery. Cell 2020;181(1):151–67.

[27] Patten DA, Wilkinson AL, O'Keeffe A, Shetty S. Scavenger receptors: novel roles in the pathogenesis of liver inflammation and cancer. Semin Liver Dis 2022;42(1):61–76.

[28] Gudgeon J, Marín-Rubio JL, Trost M. The role of macrophage scavenger receptor 1 (MSR1) in inflammatory disorders and cancer. Front Immunol 2022;13:1012002.

[29] Gong T, Tan T, Zhang P, Li H, Deng C, Huang Y, et al. Palmitic acid-modified bovine serum albumin nanoparticles target scavenger receptor-A on activated macrophages to treat rheumatoid arthritis. Biomaterials 2020;258:120296.

[30] Feng J, Xiang L, Fang C, Tan Y, Li Y, Gong T, et al. Dual-targeting of tumor cells and tumor-associated macrophages by palmitic acid modified albumin nanoparticles for antitumor and antimetastasis therapy. ACS Appl Mater Interfaces 2022;14(13):14887–902.

[31] Li L, Zhang T, Zhou L, Zhou L, Xing G, Chen Y, et al. Schisandrin B attenuates acetaminophen-induced hepatic injury through heat-shock protein 27 and 70 in mice. J Gastroenterol Hepatol 2014;29(3):640–7.

[32] Chen Q, Bao L, Lv L, Xie F, Zhou X, Zhang H, et al. Schisandrin B regulates macrophage polarization and alleviates liver fibrosis via activation of PPARγ. Ann Transl Med 2021;9(19):1500.

[33] Wang HQ, Wan Z, Zhang Q, Su T, Yu D, Wang F, et al. Schisandrin B targets cannabinoid 2 receptor in Kupffer cell to ameliorate CCl$_4$-induced liver fibrosis by suppressing NF-κB and p38 MAPK pathway. Phytomedicine 2022;98:153960.

[34] Leong PK, Ko KM. Schisandrin B: a double-edged sword in nonalcoholic fatty liver disease. Oxid Med Cell Longev 2016;2016:6171658.

[35] Nasser MI, Zhu S, Chen C, Zhao M, Huang H, Zhu P. A comprehensive review on Schisandrin B and its biological properties. Oxid Med Cell Longev 2020;2020:2172740.

[36] Cai Z, Liu J, Bian H, Cai J, Zhu G. Suppression of P2X7/NF-κB pathways by Schisandrin B contributes to attenuation of lipopolysaccharide-induced inflammatory responses in acute lung injury. Arch Pharm Res 2016;39(4):499–507.

[37] Ran J, Ma C, Xu K, Xu L, He Y, Moqbel SAA, et al. Schisandrin B ameliorated chondrocytes inflammation and osteoarthritis via suppression of NF-κB and MAPK signal pathways. Drug Des Dev Ther 2018;12:1195–204.

[38] Leong PK, Ko KM. Schisandrin B induces an Nrf2-mediated thioredoxin expression and suppresses the activation of inflammasome *in vitro* and *in vivo*. Biofactors 2015;41(5):314–23.

[39] Zhu N, Cai C, Zhou A, Zhao X, Xiang Y, Zeng C. Schisandrin B prevents hind limb from ischemia-reperfusion-induced oxidative stress and inflammation via MAPK/NF-κB Pathways in rats. Biomed Res Int 2017;2017:4237973.

[40] Checker R, Patwardhan RS, Sharma D, Menon J, Thoh M, Bhilwade HN, et al. Schisandrin B exhibits anti-inflammatory activity through modulation of the redox-sensitive transcription factors Nrf2 and NF-κB. Free Radic Biol Med 2012;53(7):1421–30.

[41] Zhang C, Li J, Xiao M, Wang D, Qu Y, Zou L, et al. Oral colon-targeted mucoadhesive micelles with enzyme-responsive controlled release of curcumin for ulcerative colitis therapy. Chin Chem Lett 2022;33(11):4924–9.

[42] Shao M, Yang W, Han G. Protective effects on myocardial infarction model: delivery of schisandrin B using matrix metalloproteinase-sensitive peptide-modified, PEGylated lipid nanoparticles. Int J Nanomedicine 2017;12:7121–30.

[43] Shao B, Tang J, Ji H, Liu H, Liu Y, Zhu D, et al. Enhanced oral bioavailability of Wurenchun (Fructus Schisandrae Chinensis extracts) by self-emulsifying drug delivery systems. Drug Dev Ind Pharm 2010;36(11):1356–63.

[44] Huang Q, Wang T, Wang HY. Ginsenoside Rb2 enhances the anti-inflammatory effect of ω-3 fatty acid in LPS-stimulated RAW264.7 macrophages by upregulating GPR120 expression. Acta Pharmacol Sin 2017;38(2):192–200.

[45] Ding Y, Zhang S, Sun Z, Tong Z, Ge Y, Zhou L, et al. Preclinical validation of silibinin/albumin nanoparticles as an applicable system against acute liver injury. Acta Biomater 2022;146:385–95.

[46] Li W, Zhou C, Fu Y, Chen T, Liu X, Zhang Z, et al. Targeted delivery of hyaluronic acid nanomicelles to hepatic stellate cells in hepatic fibrosis rats. Acta Pharm Sin B 2020;10(4):693–710.

[47] Kimbrough D, Wang SH, Wright LH, Mani SK, Kasiganesan H, LaRue AC, et al. HDAC inhibition helps post-MI healing by modulating macrophage polarization. J Mol Cell Cardiol 2018;119:51–63.

[48] Wang Z, You L, Cheng Y, Hu K, Wang Z, Cheng Y, et al. Investigation of pharmacokinetics, tissue distribution and excretion of schisandrin B in rats by HPLC-MS/MS. Biomed Chromatogr 2018;32(2):e4069.

[49] Endo Y, Kikuchi T, Nakamura M. Ornithine and histidine decarboxylase activities in mice sensitized to endotoxin, interleukin-1 or tumour necrosis factor by D-galactosamine. Br J Pharmacol 1992;107(3):888–94.

[50] Endo Y, Shibazaki M, Yamaguchi K, Kai K, Sugawara S, Takada H, et al. Enhancement by galactosamine of lipopolysaccharide (LPS)-induced tumour necrosis factor production and lethality: its suppression by LPS pretreatment. Br J Pharmacol 1999;128(1):5–12.

[51] Ma L, Zhao J, Wang J, Liu J, Duan Y, Liu H, et al. The acute liver injury in mice caused by nano-anatase TiO$_2$. Nanoscale Res Lett 2009;4(11):1275–85.

[52] Ye Y, Xu Y, Lai Y, He W, Li Y, Wang R, et al. Long non-coding RNA COX-2 prevents immune evasion and metastasis of hepatocellular carcinoma by altering M1/M2 macrophage polarization. J Cell Biochem 2018;119(3):2951–63.

[53] Lu J, Owen SC, Shoichet MS. Stability of self-assembled polymeric micelles in serum. Macromolecules 2011;44(15):6002–8.

[54] Bannon MS, Ruiz AL, Reyes KC, Marquez M. Nanoparticletracking analysis of polymer nanoparticles in blood plasma. Part Part Syst Charact 2021;38:2100016.

[55] Liu J, Zeng F, Allen C. Influence of serum protein on polycarbonate-based copolymer micelles as a delivery system for a hydrophobic anti-cancer agent. J Control Release 2005;103(2):481–97.

[56] Ge P, Yao X, Li J, Jiang R, Dai J, Zhang L. Diminazene aceturate alleviated lipopolysaccharide/D-galactosamine-induced fulminant hepatitis in mice. Biomed Pharmacother 2018;98:142–8.

[57] Sultan M, Ben-Ari Z, Masoud R, Pappo O, Harats D, Kamari Y, et al. Interleukin-1α and interleukin-1β play a central role in the pathogenesis of fulminant hepatic failure in mice. PLoS One 2017;12(9):e0184084.

[58] Zhao S, Jiang J, Jing Y, Liu W, Yang X, Hou X, et al. The concentration of tumor necrosis factor-α determines its protective or damaging effect on liver injury by regulating Yap activity. Cell Death Dis 2020;11(1):70.

[59] Pryhuber GS, Huyck HL, Roper JM, Cornejo J, O'Reilly MA, Pierce RH, et al. Acute tumor necrosis factor-alpha-induced liver injury in the absence of tumor necrosis factor receptor-associated factor 1 gene expression. Am J Pathol 2005;166(6):1637–45.

[60] Lv H, Liu Y, Zhang B, Zheng Y, Ji H, Li S. The improvement effect of gastrodin on LPS/GalN-induced fulminant hepatitis via inhibiting inflammation and apoptosis and restoring autophagy. Int Immunopharmacol 2020;85:106627.

[61] Wang K, Xiong J, Lu Y, Wang L, Tian T. SENP1-KLF4 signalling regulates LPS-induced macrophage M1-polarization. FEBS J 2023;290(1):209–24.

[62] Dixit VD, Yang H, Cooper-Jenkins A, Giri BB, Patel K, Taub DD. Reduction of T cell-derived ghrelin enhances proinflammatory cytokine expression: implications for age-associated increases in inflammation. Blood 2009;113(21):5202–5.

[63] Gao Y, Shi W, Yao H, Ai Y, Li R, Wang Z, et al. An integrative pharmacology based analysis of refined liuweiwuling against liver injury: a novel component combination and hepaprotective mechanism. Front Pharmacol 2021;12:747010.

[64] Nanji AA, Jokelainen K, Rahemtulla A, Miao L, Fogt F, Matsumoto H, et al. Activation of nuclear factor kappa B and cytokine imbalance in experimental alcoholic liver disease in the rat. Hepatology 1999;30(4):934–43.

[65] Pérez S, Rius-Pérez S. Macrophage polarization and reprogramming in acute inflammation: a redox perspective. Antioxidants 2022;11(7):1394.

[66] Jin Y, Wang H, Yi K, Lv S, Hu H, Li M, et al. Applications of nanobiomaterials in the therapy and imaging of acute liver failure. Nanomicro Lett 2020;13(1):25.